Noise in Graphene Superlattices Grown on Hexagonal Boron Nitride

Xuefei Li,[†,§] Xiaobo Lu,[‡,§] Tiaoyang Li,[†] Wei Yang,[‡] Jianming Fang,[†] Guangyu Zhang,[‡] and Yanqing Wu[*,†]

[†]Wuhan National High Magnetic Field Center and School of Electrical and Electronic Engineering, Huazhong University of Science and Technology, Wuhan 430074, China and [‡]Beijing National Laboratory for Condensed Matter Physics and Institute of Physics, Chinese Academy of Sciences, Beijing 100190, China. [§]These authors (Xuefei Li and Xiaobo Lu) contributed equally.

ABSTRACT

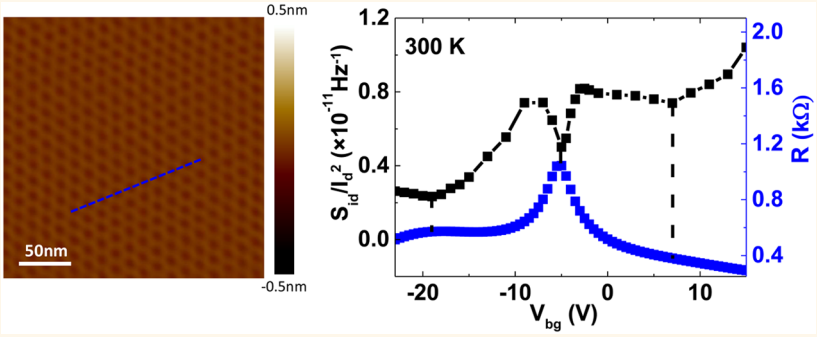

Existing in almost all electronic systems, the current noise spectral density, originated from the fluctuation of current, is by nature far more sensitive than the mean value of current, the most common characteristic parameter in electronic devices. Existing models on its origin of either carrier number or mobility are adopted in practically all electronic devices. For the past few decades, there has been no experimental evidence for direct association between 1/*f* noise and any other kinetic phenomena in solid state devices. Here, in the study of a van der Waals heterostructure of graphene on hexagonal BN superlattice, satellite Dirac points have been characterized through 1/*f* noise spectral density with pronounced local minima and asymmetric magnitude associated with its unique energy dispersion spectrum, which can only be revealed by scanning tunneling microscopy and low temperature magneto-transport measurement. More importantly, these features even emerge in the noise spectra of devices showing no minima in electric current, and are robust at all temperatures down to 4.3 K. In addition, graphene on h-BN exhibits a record low noise level of 1.6×10^{-9} μm^2 Hz^{-1} at 10 Hz, more than 1 order of magnitude lower than previous results for graphene on SiO_2. Such an epitaxial van der Waals material system not only enables an unprecedented characterization of fundamentals in solids by 1/*f* noise, but its superior interface also provides a key and feasible solution for further improvement of the noise level for graphene devices.

KEYWORDS: graphene · boron nitride · superlattice · transistor · low frequency noise

The measurement of the low-frequency noise spectra of electric current has been performed on the most common electronic devices based on semiconductors, metals, and superconductors, and practically all of these devices exhibit current noise spectral density inversely proportional to frequency, known as 1/*f* noise.[1−3] As one of the key figures-of-merit in the international technology roadmap for semiconductors (ITRS), and a limiting factor of the signal-to-noise ratio of modern nanoscale devices, 1/*f* noise has been studied extensively in Si complementary metal-oxide semiconductor (CMOS) technology. With its study, there has been a long-term effort to understand the origins of this physical parameter, and to reduce its level in modern electronics. In recent years, graphene, a monolayer of carbon atoms arranged in a honeycomb lattice, has attracted significant attention for their potential in future nanoelectronics, such as high frequency electronics and sensors.[4,5] The reduction of low-frequency noise is especially important in radio frequency applications such as voltage controlled oscillators and radar, because 1/*f* noise will be up-converted and dominate the phase noise of these circuits, limiting the their performance and reliability.[6] The study of 1/*f* noise in

* Address correspondence to yqwu@mail.hust.edu.cn.

Received for review August 22, 2015 and accepted October 4, 2015.

Published online 10.1021/acsnano.5b05283

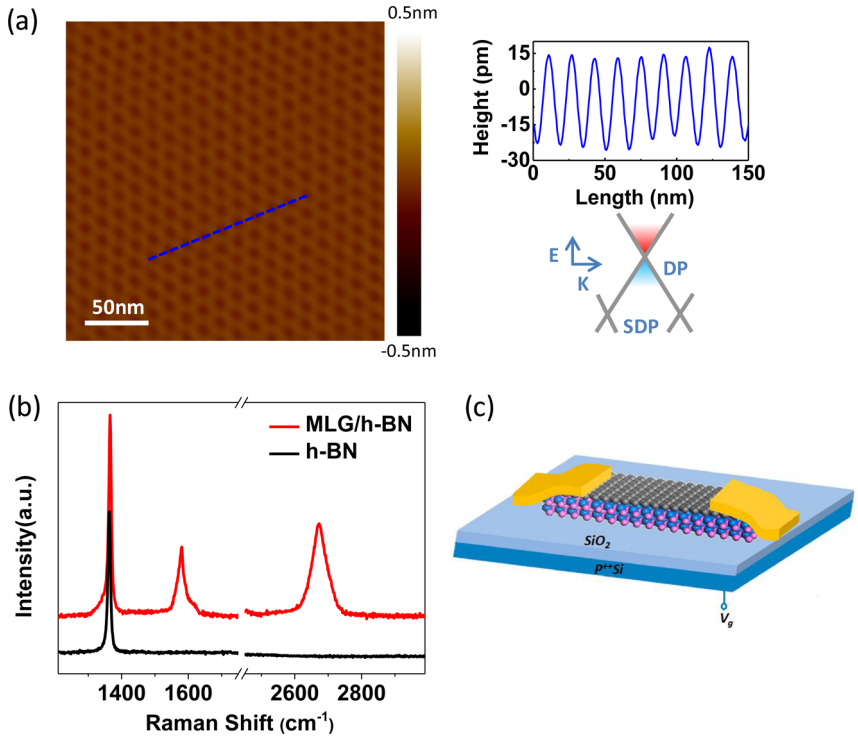

Figure 1. (a) AFM image of as-grow graphene on h-BN. It shows the well-defined moiré pattern with a periodicity of 15 ± 1 nm. Scale bars, 50 nm. The upper and lower parts in the right show the images of moiré patterns produced by graphene on h-BN and schematic of band structure of graphene epitaxially grown on h-BN, respectively. (b) Raman spectra for the as-grown graphene on h-BN (red) and h-BN surface (black). (c) A schematic of the device structure of epitaxial graphene/h-BN back-gated FETs.

graphene has been carried out extensively on graphene field-effect transistors (FETs) fabricated on SiO_2, and there is considerable understanding on the mechanisms behind its noise behavior.[7−10] Despite many efforts to improve the noise level, the normalized noise spectral density ($W \times L \times S_{id}/I_d^2$) of previous graphene devices lies in the range $\sim 10^{-8}$ to 10^{-7} μm^2 Hz^{-1} at $f = 10$ Hz, which is much higher than that of modern Si transistors.[11−15] Atomically flat hexagonal boron nitride (h-BN) has begun to attract interest first as an excellent substrate with greatly reduced scattering centers for graphene, which allows for remarkably high carrier mobility, and later, as an ultrathin dielectric for vertically sandwiched graphene heterostructures such as resonant tunneling diodes.[16−18] Very recently, van der Waals systems with superlattice structures based on graphene on h-BN with a small degree alignment have been demonstrated to create moiré patterns with altered band structure.[19−24] This new superlattice structure provides us with the unique opportunity to investigate the fundamental physics of the noise behavior at Dirac point (DP) and satellite Dirac points (SDPs) which coexist only in this system. Moreover, the noise levels of CVD epitaxial graphene on h-BN is also of great interest and has not been explored thus far.

The graphene/h-BN samples were created *via* epitaxial growth in a remote plasma system.[23] Atomic force microscopy (AFM) was used to characterize the as-grown graphene/h-BN samples. The AFM image in Figure 1a reveals a well-defined moiré pattern with a periodicity of 15 ± 1 nm, corresponding to a zero-rotation angle between the graphene and the underlying h-BN.[19,20,23] A schematic band structure for the insulating graphene/h-BN heterostructure is also shown in Figure 1a, along with the SDPs on the hole branch due to the superlattice periodic potential induced by the h-BN. The graphene lies on a dielectric composed of 100 nm SiO_2 and a 60 nm h-BN. The monolayer property of the sample is evidenced by the two characteristic peak, the G-peak (~1581 cm^{-1}) and 2D-peak (~2673 cm^{-1}), in the Raman spectrum as shown in Figure 1b. The quite weak signal of D-peak (~1345 cm^{-1}) near the characteristic peak (1367 cm^{-1}) of h-BN indicates that the sample is of high quality.[25−27] Back-gated two-terminal graphene FETs were fabricated using standard e-beam lithography and lift-off processes, and then used for current and noise measurements as shown in the schematic in Figure 1c. All characterizations were carried out in vacuum (<10^{-5} Torr) at all temperatures.

RESULTS AND DISCUSSION

The electrical transport properties of a typical graphene/h-BN superlattice sample (device 1) at room temperature, plotted in Figure 2a, show a second peak

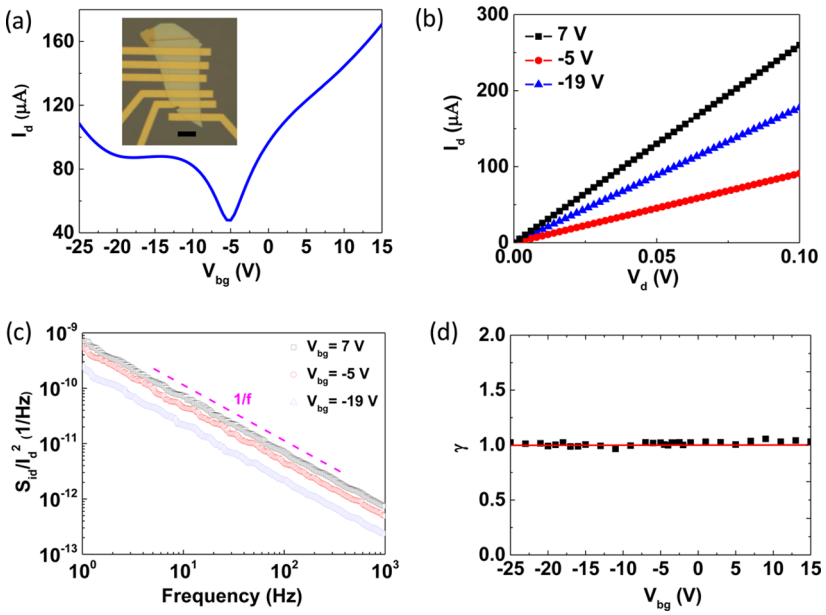

Figure 2. (a) The transfer characteristics for the graphene/h-BN sample. The inset in (a) shows an optical image of the devices and the black scale bar corresponds to 10 μm. (b) Output characteristics of the same device in (a). (c) Normalized noise spectral density as a function of frequency at three different back gate voltages. The ideal 1/*f* behavior is added for comparison. A clear 1/*f* characteristic is observed. (d) γ *versus* gate voltage V_{bg} at V_d = 50 mV at 300 K.

in the p-side current at SDP beyond the main DP in the I_d-V_g curve. Similar to that observed in previous studies, the peak in the n-side is absent unless the measurement is carried out at low temperatures due to the asymmetric bandstructure of this superlattice resulting from next-nearest-neighbor interlayer coupling.[23] The resistance peaks at $V_{bg} = -5$ V and $V_{bg} = -19$ V were attributed to the main DP and the hole side SDP, respectively. The optical image of the graphene/h-BN samples is shown in the inset of Figure 2a. Figure 2b shows the I_d-V_d output characteristics of the same device at V_{bg} = −19, −5, 7 V as shown in Figure 2a. It can be seen that the plot of the drain current I_d *versus* drain bias V_d characteristics is linear in the +100 mV voltage range. Figure 2c shows the measured low-frequency noise-normalized spectra (S_{id}/I_d^2) as a function of frequency for device 1 at V_d = 50 mV at three different gate voltages (the noise measurement setup is described in the Supporting Information). The standard method of characterizing noise in a device has been Hooge's empirical relationship:[3]

$$S_{id} = \frac{AI_d^{\beta}}{f^{\gamma}} \quad (1)$$

where S_{id} is the current noise power spectral density, f is the frequency, I_d is the current through the device channel, and A is the noise amplitude. The exponents, γ and β, are ideally expected to be close to 1 and 2, respectively. The spectra were found to be proportional to I_d^2 in the linear I_d-V_d regime and followed a 1/*f* dependence with γ = 1.03 + 0.01. All the measured devices exhibit the same behavior with the exponents close to the ideal γ = 1, as shown in Figure 2d. This suggests that the 1/*f* noise in the graphene/h-BN samples is caused by a collection of fluctuations in the resistance with a wide distribution of time constant.[12]

The resistance R as a function of V_{bg} for four different FETs at 300 K is shown in Figure 3a−d. We arrange the four devices measured in a fashion such that the left SDP of device 1 (Figure 3a) is most pronounced, and it gradually becomes negligible from device 1 to device 4 (Figure 3d). For the device with visible SDP, the voltage difference between the SDP and DP can be estimated using $\Delta V_g = \pi e/(\lambda^2 C_g)$,[23] where λ is the superlattice period. Given that λ = 13.6 nm and the capacitance per unit area C_g = 21.79 nF/cm^2, we can calculate ΔV_g = 12.5 V, which is close to our experimentally measured 14 V in the hole side. Figure 3e−h shows the dependence of the normalized noise spectral density S_{id}/I_d^2 at f = 100 Hz on V_{bg} for the corresponding devices. It is obvious that the 1/*f* noise for all devices exhibits a pronounced local minimum at about $V_{bg} = -5$ V, close to the DPs as shown by the dashed lines. Meanwhile, there are two extra minima on either side of the DP. The voltage differences of the left and right minima to the DP are 14 and 12 V, respectively, corresponding to the voltage differences ΔV_g between the DP and SDPs as mentioned earlier. As such, the three valleys of the S_{id}/I_d^2 curves in Figure 3e−h closely coincide with the two SDPs and the DP as shown in Figure 3a−d. Although the coupling between graphene and h-BN gives rise to new Dirac points near the edges of the superlattice Brillouin zone and creates superlattice minibands,[28−30] there has been no experimental observations of major energy gaps at the SDPs so far.[31] As shown in experimental observations, both electron

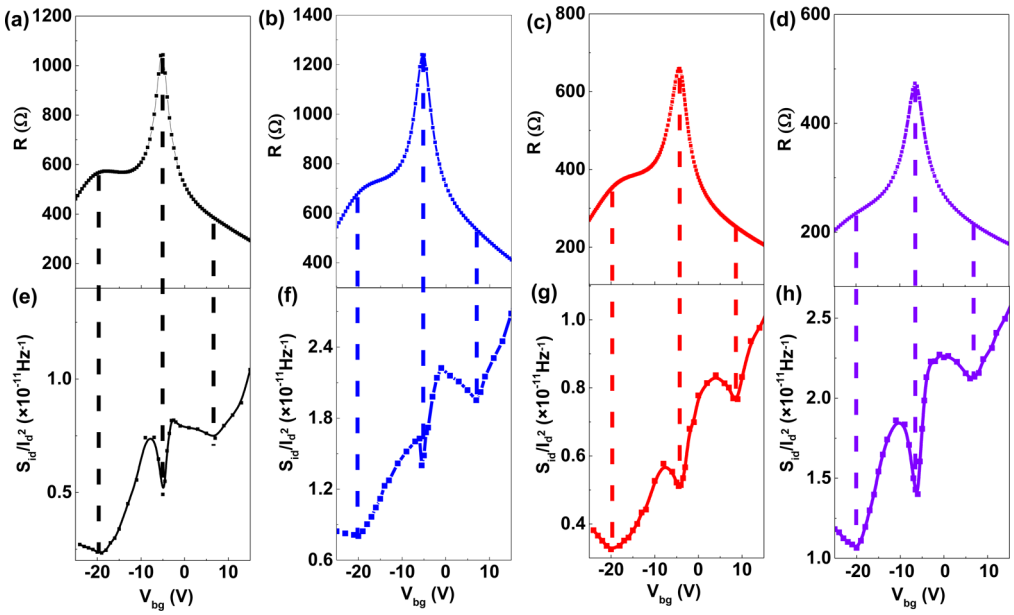

Figure 3. (a−d) Resistance *versus* applied gate voltage (V_{bg}) for four different graphene/h-BN samples at room temperature. (e−h) Current spectral density S_{id}/I_d^2 at $f = 100$ Hz *versus* back gate voltage V_{bg} for the corresponding FETs. The dotted lines show that the resistance peaks in panels a−d coincide with the $(S_{id}/I_d^2)_{min}$ in the panels e−h.

and holes coexists at SDPs.[21] At the left SDP (the noise at the right SDP could be explained similarly), both of holes and electrons contribute to noise and the residual charges provide effective screening to the trap charges. When the gate bias moves away from the left SDP, holes (electrons for $V_g - V_{left\text{-}SDP} > 0$) would dominate the electrons (holes) and an increase of noise from electrons (holes) is greater than a decrease of noise from holes (electrons).[8] Therefore, local noise minima have been observed at the SDPs. Surprisingly, the noise minima at the right SDPs are clearly visible on each device, whereas the *IV* data shows no dips at corresponding positions. Moreover, device 4 exhibits almost identical *IV* curve as conventional graphene FETs, but strikingly different noise spectra with a dip at each SDP. These features demonstrate not only the sensitive nature of the noise spectra measurement, but also its direct dependence on the fundamental electronic structure of the moiré pattern associated only with energy dispersion spectrum.

To further investigate the noise spectral density and its relation with DC current, Figure 4a plots the drain current asymmetry $[(I_{d\ right\text{-}SDP} - I_{d\ left\text{-}SDP})/I_{d\ left\text{-}SDP}]$ and noise level asymmetry $\{[(S_{id}/I_d^2{}_{right\text{-}SDP}) - (S_{id}/I_d^2{}_{left\text{-}SDP})]/(S_{id}/I_d^2{}_{left\text{-}SDP})\}$ at the SDPs for four devices. In addition to the emergence of local valleys, the asymmetry in the noise level is much more pronounced than that of electric current, which is almost four times larger typically and up to 20 times larger in the case of device 4. The two most common models for conventional noise spectra, namely the Hooge model and McWorther model, rely either on the mobility or carrier number, and should be very similar to electric current. However, the asymmetry difference between noise spectral density and electric current in this superlattice system indicates that neither of the two models can explain the physical origin. This noise level asymmetry is associated with the breaking of electron−hole symmetry by next-nearest-neighbor interlayer coupling, and has a large effect compared to carrier number or mobility.

Furthermore, in order to benchmark the noise level in this structure with previous graphene devices, as well as the potential for further improvement, the mobility dependence of the noise level is studied. The field-effect mobility μ_{FE} of the four devices is extracted in the linear region of the transfer characteristics according to the following equation $\mu_{FE} = g_m/(C_g EW)$, where W is the width of the channel, E is the transverse electric field in the channel, and g_m is the transconductance.[32] The field-effect mobility of samples from device 1 to device 4 was found to be 2643, 2124, 1620, and 1272 cm^{-2} V^{-1} s^{-1}, respectively. It is noted here that due to the crystal defects induced during the CVD growth, the mobility here has much room for further improvement. We plot the area normalized noise spectral density ($W \times L \times S_{id}/I_d^2$) at the DP and two SDPs as a function of mobility. As seen in Figure 4b, the noise level exhibits a monotonic trend that decreases slightly with increasing mobility at the DP and two SDPs, which shows the great potential for further improvement in noise level as growth techniques for higher mobility are optimized. As one of the most accepted benchmarking strategies, we recorded the area dependence of noise spectral density, S_{id}/I_d^2 from the most representative monolayer graphene FETs reported over the past few years in the literature as shown in Figure 4c. Compared to graphene

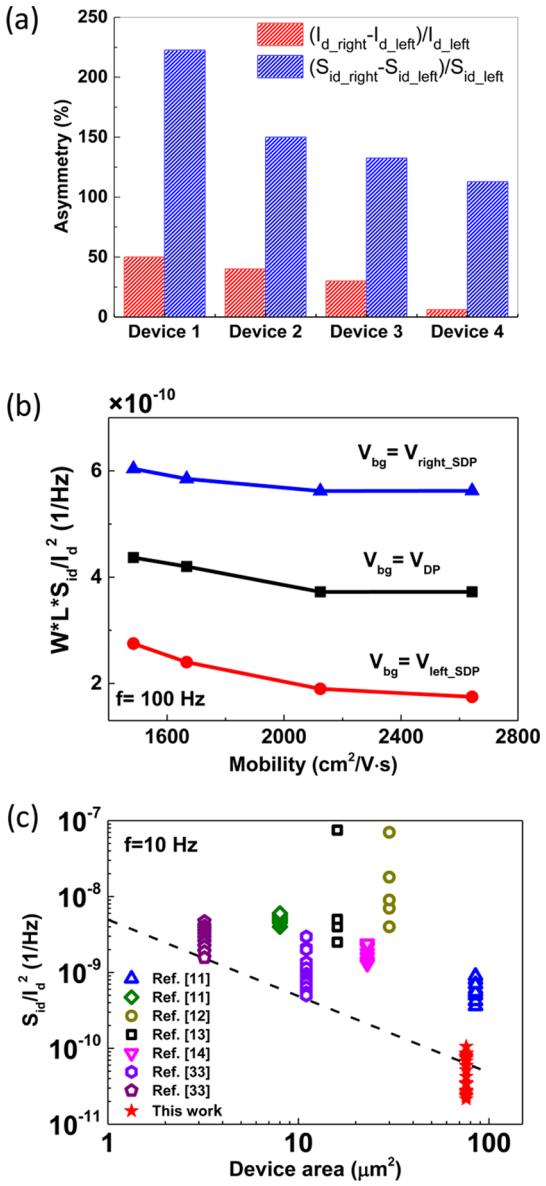

Figure 4. (a) Asymmetry in drain current (($I_{d\ right\text{-}SDP} - I_{d\ left\text{-}SDP}$)/$I_{d\ left\text{-}SDP}$) (red) and noise level {[($S_{id}/I_d^2{}_{right\text{-}SDP}$) − ($S_{id}/I_d^2{}_{left\text{-}SDP}$)]/($S_{id}/I_d^2{}_{left\text{-}SDP}$)} (blue) at the two SDPs for four different devices at room temperature. (b) Area normalized noise spectral density ($W \times L \times S_{id}/I_d^2$) as a function of mobility at the DP and two SDPs. (c) Current spectral density S_{id}/I_d^2 *versus* channel area for different FETs.

FETs with SiO_2 gate dielectrics, the device reported here exhibits an extremely low noise level up to 1.6×10^{-9} μm^2 Hz^{-1} at 10 Hz at room temperature, which is more than an order of magnitude lower than the previous graphene FETs.[11−14] This is consistent with recently reported results from the BN/graphene/BN transistors,[33] due to the fact that the surface of the h-BN substrate is ultraflat and free of dangling bonds, greatly reducing the numbers of charge traps compared with SiO_2 and leading to a strong decrease of device noise level.[16,19,24,34] Compared with the high mobility in the mechanically transferred exfoliated samples, it should be noted that the mobility in our

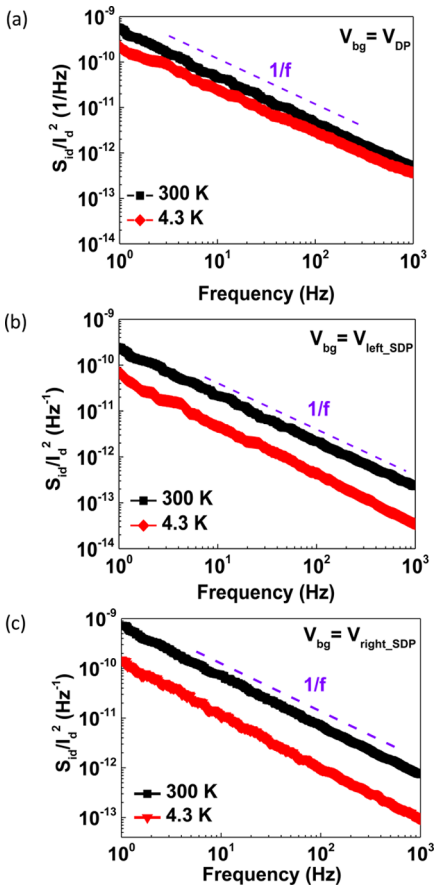

Figure 5. (a) Normalized noise spectral density (S_{id}/I_d^2) as a function of frequency with $V_{bg} = V_{DP}$ at various temperatures. (b) Normalized noise spectral density (S_{id}/I_d^2) as a function of frequency with $V_{bg} = V_{left\text{-}SDP}$ at different temperatures. (c) Normalized noise spectral density (S_{id}/I_d^2) as a function of frequency with $V_{bg} = V_{right\text{-}SDP}$ at various temperature. The dotted lines in panels a−c show the ideal 1/*f* behavior.

samples is mainly limited by the graphene defectively instead of graphene/h-BN interface states. This further suggests that the low frequency noise behavior in our structure originates from the moiré pattern of graphene, induced by the underlying h-BN, instead of the graphene sheet itself. The record low noise level suggests that it is beneficial to employ a crystalline h-BN substrate to reduce noise in graphene transistors.

To further investigate the origins of the noise in the epitaxial graphene/h-BN superlattice, we carried out 1/*f* noise measurement from 300 to 4.3 K for the device 1. The normalized noise spectral density S_{id}/I_d^2 as a function of frequency at $V_{bg} = V_{DP}$, $V_{bg} = V_{left\_\ SDP}$, and $V_{bg} = V_{right\_SDP}$ for different temperatures with V_d = 50 mV are shown in Figure 5a−c, respectively. It can be seen that the noise level decreases with lowering temperature for both cases, indicating a thermal activation process. The noise followed the 1/*f* trend at all temperatures without an emergence of generation-recombination bulge signatures.

Figure 6a,b shows the resistance of the same device as a function of V_{bg} at V_d = 50 mV with 300 and 4.3 K,

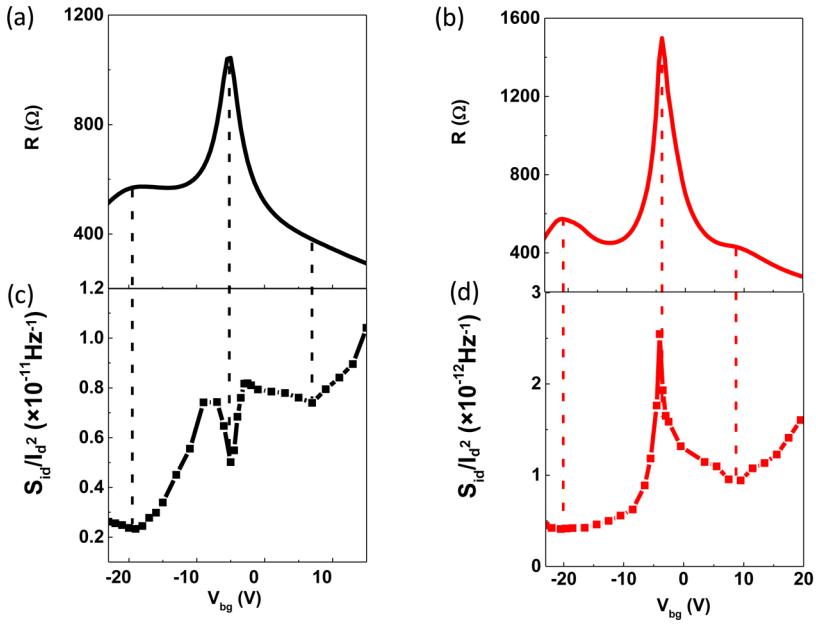

Figure 6. (a and b) Resistance *versus* applied gate voltage (V_{bg}) for device 1 at 300 and 4.3 K. (c and d) Current spectral density S_{id}/I_d^2 at $f = 100$ Hz *versus* back gate voltage V_{bg} for the same device at the corresponding temperature. The dotted lines show that the resistance peaks in panels a and b coincide with the $(S_{id}/I_d^2)_{min}$ in panels c and d.

respectively. In addition to the usual resistance peak associated with the DP located at $V_{bg} = -5$ V, two additional satellite peaks at both sides of the DP appear pronounced at decreasing temperature. The satellite peak in the hole side is always stronger than that in the electron side, which can be attribute to the next-nearest-neighbor interlayer coupling as mentioned earlier.[23] Figure 6c,d plots the noise spectral density S_{id}/I_d^2 for the same device as functions of V_{bg} accordingly at different temperatures. It is clearly seen that the noise minimum ($(S_{id}/I_d^2)_{min}$) coincides with the resistance maximum (R_{peak}) at all temperatures at SDPs, which is consistent with the results in Figure 3. At the DP, the noise level exhibits an *M*-shape gate-bias dependence at 300 K as explained above. At even lower temperatures, the shape drastically changes into Λ-shape behavior, consistent with previous papers.[10,35] This is due to the fact that some active traps may have been frozen and electrons could better screen the potential fluctuation, which results in the change of noise behavior from *M*-shape to Λ-shape. However, the *V*-shape noise behavior remains unchanged at all temperatures, indicating that either the electronic screening effect insignificant, or the active traps do not reside near the SDP energy level. In addition, the noise level of the left SDP is always smaller than that of the right SDP, which is independent of temperature, and consistent with the results in Figure 3.

CONCLUSIONS

In conclusion, in this study of graphene superlattice grown on hexagonal boron nitride, the current noise spectral density exhibits pronounced local minima at the SDPs, and more importantly, these features even emerge when there are no corresponding resistance maxima, and are robust down to 4.3 K. Moreover, at the SDPs, the noise spectra show enhanced asymmetries between electron and hole branches, almost 18 times larger the differences in conductance. These results originate from the unique energy dispersion spectrum of the superlattice, which was revealed previously by scanning tunneling microscopy and low temperature magneto-transport measurement. Moreover, graphene on h-BN exhibits a record low noise level of 1.6×10^{-9} μm^2 Hz^{-1} at 10 Hz, nearly 60 times lower than previous results from graphene on SiO_2. Such an epitaxial van der Waals material system not only provides a unique opportunity for the direct link between noise spectra and fundamental electronic structures, but its superior interface also provides a key and feasible solution for further improvement of the noise level in graphene devices.

METHODS

The graphene/h-BN samples were obtained by the epitaxial growth approach in a remote plasma system. The ~60 nm single crystal h-BN flakes were mechanically exfoliated on a 100 nm-thick SiO_2 substrate. During the growth period, the methane (CH_4) is dissociated into reactive radicals in a radio frequency electric field, thus realizing a low temperature (~500 °C) growth. The standard electron beam lithography process was applied to define the electrode pattern, followed by electron beam evaporation of 120 nm-Au/5 nm-Pd as the contact metal. After a standard metal lift-off process, the device

was annealed in an argon atmosphere at 250 °C for 2 h. The DC measurement was carried out in a lakeshore cryogenic probe station under vacuum ($<10^{-5}$ Torr) using an Agilent B1500A parameter analyzer. The low frequency 1/*f* noise measurements were carried out by Agilent E4725A 1/*f* noise system with an Agilent E5052B.

Conflict of Interest: The authors declare no competing financial interest.

Supporting Information Available: The Supporting Information is available free of charge on the ACS Publications website at DOI: 10.1021/acsnano.5b05283.

Information on the of noise measurement setup, current noise power spectral density for different V_d, and current noise spectral density of three FETs (PDF)

Acknowledgment. This project was supported by the Natural Science Foundation of China (Grant Nos. 11404118 and 61390504).

REFERENCES AND NOTES

1. Dutta, P.; Horn, P. M. Low-Frequency Fluctuations in Solids: 1/*f* Noise. *Rev. Mod. Phys.* **1981**, *53*, 497–516.
2. Weissman, M. B. 1/*f* Noise and Other Slow, Nonexponential Kinetics in Condensed Matter. *Rev. Mod. Phys.* **1988**, *60*, 537–571.
3. Hooge, F. 1/*f* Noise Sources. *IEEE Trans. Electron Devices* **1994**, *41*, 1926–1935.
4. Schedin, F.; Geim, A.; Morozov, S.; Hill, E.; Blake, P.; Katsnelson, M.; Novoselov, K. Detection of Individual Gas Molecules Adsorbed on Graphene. *Nat. Mater.* **2007**, *6*, 652–655.
5. Wu, Y.; Lin, Y.-m.; Bol, A. A.; Jenkins, K. A.; Xia, F.; Farmer, D. B.; Zhu, Y.; Avouris, P. High-Frequency, Scaled Graphene Transistors on Diamond-Like Carbon. *Nature* **2011**, *472*, 74–78.
6. Razavi, B. A Study of Phase Noise in CMOS Oscillators. *IEEE J. Solid-State Circuits* **1996**, *31*, 331–343.
7. Heller, I.; Chatoor, S.; Männik, J.; Zevenbergen, M. A. G.; Oostinga, J. B.; Morpurgo, A. F.; Dekker, C.; Lemay, S. G. Charge Noise in Graphene Transistors. *Nano Lett.* **2010**, *10*, 1563–1567.
8. Xu, G.; Torres, C. M., Jr; Zhang, Y.; Liu, F.; Song, E. B.; Wang, M.; Zhou, Y.; Zeng, C.; Wang, K. L. Effect of Spatial Charge Inhomogeneity on 1/*f* Noise Behavior in Graphene. *Nano Lett.* **2010**, *10*, 3312–3317.
9. Zhang, Y.; Mendez, E. E.; Du, X. Mobility-Dependent Low-Frequency Noise in Graphene Field-Effect Transistors. *ACS Nano* **2011**, *5*, 8124–8130.
10. Kaverzin, A.; Mayorov, A. S.; Shytov, A.; Horsell, D. Impurities as a Source of 1/*f* Noise in Graphene. *Phys. Rev. B: Condens. Matter Mater. Phys.* **2012**, *85*, 075435.
11. Rumyantsev, S.; Liu, G.; Stillman, W.; Shur, M.; Balandin, A. Electrical and Noise Characteristics of Graphene Field-Effect Transistors: Ambient Effects, Noise Sources and Physical Mechanisms. *J. Phys.: Condens. Matter* **2010**, *22*, 395302.
12. Balandin, A. A. Low-Frequency 1/*f* Noise in Graphene Devices. *Nat. Nanotechnol.* **2013**, *8*, 549–555.
13. Liu, G.; Rumyantsev, S.; Shur, M.; Balandin, A. A. Graphene Thickness-Graded Transistors with Reduced Electronic Noise. *Appl. Phys. Lett.* **2012**, *100*, 033103.
14. Liu, G.; Rumyantsev, S.; Shur, M. S.; Balandin, A. A. Origin of 1/*f* Noise in Graphene Multilayers: Surface vs. Volume. *Appl. Phys. Lett.* **2013**, *102*, 093111.
15. Hossain, M. Z.; Rumyantsev, S.; Shur, M. S.; Balandin, A. A. Reduction of 1/*f* Noise in Graphene after Electron-Beam Irradiation. *Appl. Phys. Lett.* **2013**, *102*, 153512.
16. Dean, C.; Young, A.; Meric, I.; Lee, C.; Wang, L.; Sorgenfrei, S.; Watanabe, K.; Taniguchi, T.; Kim, P.; Shepard, K.; et al. Boron Nitride Substrates for High-Quality Graphene Electronics. *Nat. Nanotechnol.* **2010**, *5*, 722–726.
17. Britnell, L.; Gorbachev, R.; Jalil, R.; Belle, B.; Schedin, F.; Mishchenko, A.; Georgiou, T.; Katsnelson, M.; Eaves, L.; Morozov, S.; et al. Field-Effect Tunneling Transistor Based on Vertical Graphene Heterostructures. *Science* **2012**, *335*, 947–950.
18. Mishchenko, A.; Tu, J.; Cao, Y.; Gorbachev, R.; Wallbank, J.; Greenaway, M.; Morozov, V.; Morozov, S.; Zhu, M.; Wong, S.; et al. Twist-Controlled Resonant Tunnelling in Graphene/Boron Nitride/Graphene Heterostructures. *Nat. Nanotechnol.* **2014**, *9*, 808–813.
19. Xue, J.; Sanchez-Yamagishi, J.; Bulmash, D.; Jacquod, P.; Deshpande, A.; Watanabe, K.; Taniguchi, T.; Jarillo-Herrero, P.; LeRoy, B. J. Scanning Tunnelling Microscopy and Spectroscopy of Ultra-Flat Graphene on Hexagonal Boron Nitride. *Nat. Mater.* **2011**, *10*, 282–285.
20. Yankowitz, M.; Xue, J.; Cormode, D.; Sanchez-Yamagishi, J. D.; Watanabe, K.; Taniguchi, T.; Jarillo-Herrero, P.; Jacquod, P.; LeRoy, B. J. Emergence of Superlattice Dirac Points in Graphene on Hexagonal Boron Nitride. *Nat. Phys.* **2012**, *8*, 382–386.
21. Ponomarenko, L.; Gorbachev, R.; Yu, G.; Elias, D.; Jalil, R.; Patel, A.; Mishchenko, A.; Mayorov, A.; Woods, C.; Wallbank, J.; et al. Cloning of Dirac Fermions in Graphene Superlattices. *Nature* **2013**, *497*, 594–597.
22. Dean, C. R.; Wang, L.; Maher, P.; Forsythe, C.; Ghahari, F.; Gao, Y.; Katoch, J.; Ishigami, M.; Moon, P.; Koshino, M.; Taniguchi, T.; Watanabe, K.; Shepard, K. L.; Hone, J.; Kim, P.; et al. Hofstadter's Butterfly and the Fractal Quantum Hall Effect in Moire Superlattices. *Nature* **2013**, *497*, 598–602.
23. Yang, W.; Chen, G.; Shi, Z.; Liu, C.-C.; Zhang, L.; Xie, G.; Cheng, M.; Wang, D.; Yang, R.; Shi, D.; et al. Epitaxial Growth of Single-Domain Graphene on Hexagonal Boron Nitride. *Nat. Mater.* **2013**, *12*, 792–797.
24. Decker, R.; Wang, Y.; Brar, V. W.; Regan, W.; Tsai, H.-Z.; Wu, Q.; Gannett, W.; Zettl, A.; Crommie, M. F. Local Electronic Properties of Graphene on a BN Substrate *via* Scanning Tunneling Microscopy. *Nano Lett.* **2011**, *11*, 2291–2295.
25. Ferrari, A.; Meyer, J.; Scardaci, V.; Casiraghi, C.; Lazzeri, M.; Mauri, F.; Piscanec, S.; Jiang, D.; Novoselov, K.; Roth, S.; et al. Raman Spectrum of Graphene and Graphene Layers. *Phys. Rev. Lett.* **2006**, *97*, 187401.
26. Malard, L.; Pimenta, M.; Dresselhaus, G.; Dresselhaus, M. Raman Spectroscopy in Graphene. *Phys. Rep.* **2009**, *473*, 51–87.
27. Dresselhaus, M. S.; Jorio, A.; Hofmann, M.; Dresselhaus, G.; Saito, R. Perspectives on Carbon Nanotubes and Graphene Raman Spectroscopy. *Nano Lett.* **2010**, *10*, 751–758.
28. Sławińska, J.; Zasada, I.; Klusek, Z. Energy Gap Tuning in Graphene on Hexagonal Boron Nitride Bilayer System. *Phys. Rev. B: Condens. Matter Mater. Phys.* **2010**, *81*, 155433.
29. Wallbank, J. R.; Patel, A. A.; Mucha-Kruczyński, M.; Geim, A. K.; Fal'ko, V. I. Generic Miniband Structure of Graphene on a Hexagonal Substrate. *Phys. Rev. B: Condens. Matter Mater. Phys.* **2013**, *87*, 245408.
30. Song, J. C. W.; Shytov, A. V.; Levitov, L. S. Electron Interactions and Gap Opening in Graphene Superlattices. *Phys. Rev. Lett.* **2013**, *111*, 266801.
31. Chen, Z.-G.; Shi, Z.; Yang, W.; Lu, X.; Lai, Y.; Yan, H.; Wang, F.; Zhang, G.; Li, Z. Observation of an Intrinsic Bandgap and Landau Level Renormalization in Graphene/Boron-Nitride Heterostructures. *Nat. Commun.* **2014**, *5*, 5.
32. Sze, S. M.; Ng, K. K. *Physics of Semiconductor Devices*; John Wiley & Sons: New York, 2006.
33. Stolyarov, M. A.; Liu, G.; Rumyantsev, S. L.; Shur, M.; Balandin, A. A. Suppression of 1/*f* Noise in Near-Ballistic h-BN-Graphene-h-BN Heterostructure Field-Effect Transistors. *Appl. Phys. Lett.* **2015**, *107*, 023106.
34. Wang, B. C.; Wu, S. L.; Lu, Y. Y.; Chang, S. J.; Chen, J. F.; Tsai, S. C.; Hsu, C. H.; Yang, C. W.; Chen, C. G.; Cheng, O.; et al. Comparison of the Trap Behavior between ZrO_2 and HfO_2 Gate Stack nMOSFETs by 1/*f* Noise and Random Telegraph Noise. *IEEE Electron Device Lett.* **2013**, *34*, 151–153.
35. Pal, A. N.; Ghosh, A. Ultralow Noise Field-Effect Transistor from Multilayer Graphene. *Appl. Phys. Lett.* **2009**, *95*, 082105.